Analogy Between the "Hidden Order" and the Orbital Antiferromagnetism in $URu_{2-x}Fe_xSi_2$

H.-H. Kung,[1,*] S. Ran,[2,3] N. Kanchanavatee,[2,3] V. Krapivin,[1] A. Lee,[1] J. A. Mydosh,[4] K. Haule,[1] M. B. Maple,[2,3] and G. Blumberg[1,5,†]

[1]*Department of Physics & Astronomy, Rutgers University, Piscataway, New Jersey 08854, USA*
[2]*Department of Physics, University of California San Diego, La Jolla, California 92093, USA*
[3]*Center for Advanced Nanoscience, University of California San Diego, La Jolla, California 92093, USA*
[4]*Kamerlingh Onnes Laboratory, Leiden University, 2300 RA Leiden, The Netherlands*
[5]*National Institute of Chemical Physics and Biophysics, 12618 Tallinn, Estonia*

(Received 29 August 2016; published 22 November 2016)

We study $URu_{2-x}Fe_xSi_2$, in which two types of staggered phases compete at low temperature as the iron concentration x is varied: the nonmagnetic "hidden order" (HO) phase below the critical concentration x_c, and unconventional antiferromagnetic (AFM) phase above x_c. By using polarization resolved Raman spectroscopy, we detect a collective mode of pseudovectorlike A_{2g} symmetry whose energy continuously evolves with increasing x; it monotonically decreases in the HO phase until it vanishes at $x = x_c$, and then reappears with increasing energy in the AFM phase. The mode's evolution provides direct evidence for a unified order parameter for both nonmagnetic and magnetic phases arising from the orbital degrees-of-freedom of the uranium-5f electrons.

DOI: 10.1103/PhysRevLett.117.227601

URu_2Si_2 holds long-standing interest in the strongly correlated electron community due to several emergent types of long range orders it exhibits. Below the second order phase transition temperature $T_{DW}(x)$, two density-wave-like phases involving long range ordering of the uranium-5f electrons compete when a critical parameter x is tuned [1], where x can be chemical substituent concentration [2,3], pressure [4,5], or magnetic field [6,7]. At $x < x_c$, the system settles in the enigmatic "hidden order" (HO) phase [8–10], which transforms into an unconventional large moment antiferromagnetic (LMAF) phase through a first order transition for $x > x_c$. At low temperature below 1.5 K, a superconducting state, which likely breaks time reversal symmetry [11], emerges from the HO phase.

Recently, much effort has been dedicated towards unraveling the order parameter of the HO phase through several newly developed experimental and theoretical techniques [11–16]. In particular, the symmetry analysis of the low temperature Raman scattering data implies that the reflection symmetries of tetragonal D_{4h} point group (No. 139 $I4/mmm$) associated with the paramagnetic (PM) state are broken, and that a chirality density wave emerges as the HO ground state [17].

The HO and LMAF phases are known to exhibit "adiabatic continuity" [18]; i.e., both phases possess similar electronic properties [2,19], and the Fermi surface practically shows no change across the phase boundary [18]. Furthermore, inelastic neutron scattering observed a dispersive collective excitation in the HO phase [5,20] and recently in the LMAF phase of pressurized URu_2Si_2 [21]. This raises the intriguing question of the symmetry relation between the two phases. However, experimental progress is hindered due to inherent constraints of low temperature pressurized experiments.

The availability of $URu_{2-x}Fe_xSi_2$ crystals [2,3] made it possible to perform high-resolution spectroscopic experiments at low temperature and ambient pressure in both the HO and LMAF phases. Iron substitution mimics the effect of applying small pressure or in-plane stress on the URu_2Si_2 lattice, and the iron (Fe) concentration, x, can be approximately treated as an effective "chemical pressure" [2]. Recently, the phase diagram of $URu_{2-x}Fe_xSi_2$ single crystals have been determined [1,3,22–24], which resembles the low pressure phase diagram of pristine URu_2Si_2 [4,16] [Fig. 1(a)]. The inelastic neutron scattering measurements again illustrate the analogies of the LMAF phase to the HO phase [24,25], albeit differences remain relating to the existence of the resonance in the LMAF state of pressurized [21,25] or Fe-substituted crystals [24].

In this Letter, we study the dynamical fluctuations between the competing nonmagnetic HO and the time-reversal-symmetry breaking LMAF ground states in $URu_{2-x}Fe_xSi_2$ as a function of x using polarization resolved Raman spectroscopy [28]. Albeit the distinct discrete symmetries are broken above and below the critical concentration x_c, we detect a collective mode continuously evolving with parameter x in the pseudovectorlike A_{2g} symmetry channel. In the HO phase, the mode energy decreases as x is increased, disappearing at the critical Fe concentration x_c. In the LMAF phase, the collective mode again emerges in the same A_{2g} symmetry channel with the energy increasing with x. The continuous transformation of this collective excitation, a photoinduced transition between the HO and LMAF electronic phases, provides direct

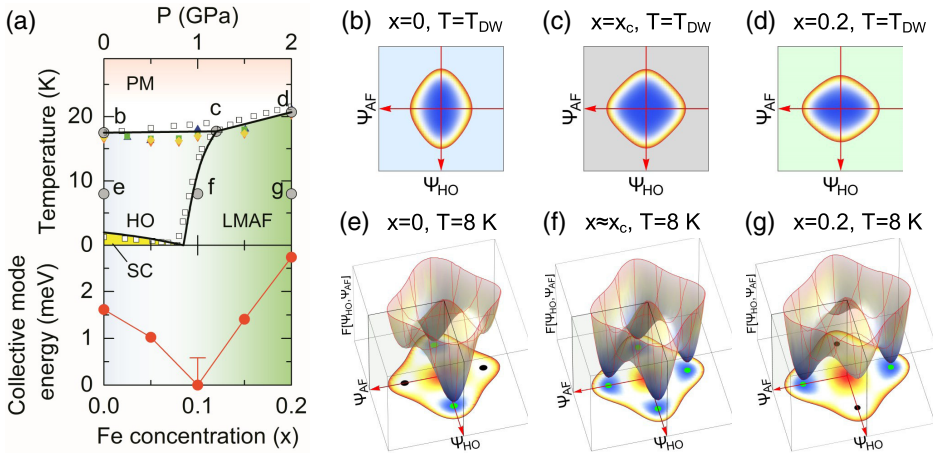

FIG. 1. (a) The upper panel shows the phase diagram of URu_2Si_2 system, where the black lines show the phase boundaries. The measurements on the iron substituted $URu_{2-x}Fe_xSi_2$ crystals from neutron diffraction [22] (blue triangle), electrical resistivity [2] (green square), magnetic susceptibility [2] (purple triangle), and heat capacity [3] (yellow diamond), are overlaid with the neutron diffraction results for URu_2Si_2 under hydrostatic pressure [4] (open square) to show the similarity between the two tuning parameters. The lower panel shows the dependence of the A_{2g} collective mode energy on the Fe concentration, x [Fig. 2]. At the critical concentration, $x = 0.1$, the mode maximum is below the accessible energy cutoff. Therefore, the data point is placed at zero energy, with the error bar reflecting the instrumental cutoff. (b)–(g) Schematics of the Ginzburg-Landau free energy in Eq. (1) at various special points in the phase diagram [solid gray circles in (a)]. ψ_{HO} and ψ_{AFM} are the real and imaginary part of the hexadecapole order parameter, respectively [26,27].

experimental evidence for a unified order parameter for both nonmagnetic and magnetic phases arising from the orbital degree of freedom of the uranium-5f electrons.

The polarized Raman spectra were acquired in a quasibackscattering geometry from the ab surface of $URu_{2-x}Fe_xSi_2$ single crystals grown by the Czochralski method [28]. We use 752.5 nm line of a Kr^+ laser for excitation. The scattered light was analyzed by a custom triple-grating spectrometer. The laser spot size on the sample is roughly $50 \times 100\ \mu m^2$. The power on the sample is about 12 mW for most temperatures, and kept below 6 mW to achieve the lowest temperatures.

Figure 2 shows the temperature dependence of the Raman response in the eminent A_{2g} symmetry channel of the D_{4h} group, which transforms as a pseudovector [29]. The upper panels show the intensity plots of the low energy Raman response $\chi''_{A2g}(\omega, T)$ below 30 K. Above $T_{\mathrm{DW}}(x)$, a quasielastic peak (QEP) comprises most of the spectral weight for all samples, narrowing towards the transition. The observed QEP originates from overdamped excitations between quasidegenerate crystal field states [17,26], and the narrowing of the QEP with cooling is due to the increase of excitation lifetime, related to the development of a hybridization gap and formation of a heavy Fermi liquid [30,31].

Below $T_{\mathrm{DW}}(x)$, the most significant feature in the A_{2g} channel is a sharp collective mode. The sharpness of this resonance suggests the lack of relaxation channels due to the opening of an energy gap [1,30,32]. In order to see the

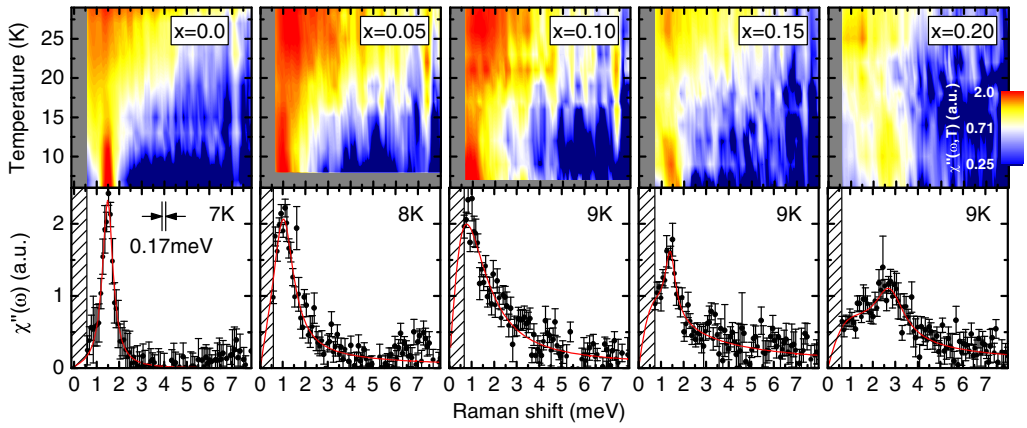

FIG. 2. Low temperature Raman response in the A_{2g} symmetry channel, $\chi''_{A2g}(\omega, T)$ [28]. The upper panels show intensity plots, where the intensities are color coded in logarithmic scale. The lower panels show the spectra at about half the transition temperature to emphasize the collective mode, where the error bars represent one standard deviation, and the red solid lines are guides to the eye. The energies of this mode as function of the Fe concentration x are shown in Fig. 1(a).

mode's line shape more clearly, we plot $\chi''_{A2g}(\omega, T)$ for each Fe concentration x in the lower panels, with $T \approx T_{\mathrm{DW}}(x)/2$. The line shapes broaden with increasing x owing to the inhomogeneity of the local stress field, or unsuppressed relaxation channels introduced by doping that interact with the collective mode, which may also be related to the increasing continuum in the $x = 0.15$ and 0.2 spectra. In contrast to the monotonic broadening of the line-shape width, the collective mode frequency shows nonmonotonic behavior as function of x. The mode energy versus Fe concentration x is shown in the lower panel of Fig. 1(a). The energy decreases with increasing x in the HO phase, until it vanishes below the instrumental resolution at $x = 0.10$, which is close to the HO and LMAF phase boundary determined by elastic neutron scattering [22] and thermal expansion measurements [3]. The resonance reappears in the LMAF phase, where the energy increases with increasing x. The resonance in the LMAF state appears in the same A_{2g} symmetry channel as the collective mode in the HO phase.

The similarity of the Raman response in the HO and LMAF phases encourages us to compare our results with the magnetic susceptibility. Figure 3 shows the temperature dependence of the real part of the static A_{2g} Raman susceptibility $\chi_{A2g}(0, T)$, compared with the c-axis magnetic susceptibility $\chi_c^m(T)$ [3]. While there are discrepancies around the maxima at about 50–100 K, both quantities follow the same Curie-Weiss-like temperature dependence above 100 K, followed by a suppression approaching the second order phase transition.

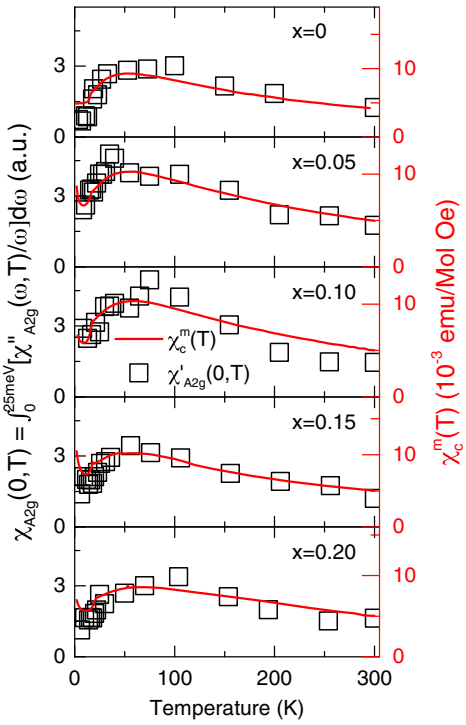

FIG. 3. The static Raman susceptibility in the A_{2g} symmetry channel (open squares) $\chi_{A2g}(0, T)$, compared with the magnetic susceptibility with field applied along the c axis [3] (solid line).

The comparison between $\chi_{A2g}(0, T)$ and $\chi_c^m(T)$ has been studied within the frame work of a phenomenological minimal model [17,26]. The model is composed of two low-laying singlet orbital levels on uranium sites as suggested by recent experiment [33], separated by small energy ω_0. These states with pseudovectorlike A_{2g} and full-symmetric A_{1g} symmetries are denoted by $|A_{2g}\rangle$ and $|A_{1g}\rangle$, respectively. At high temperatures, the crystal field states are quasidegenerate in energy and localized at the uranium f shells in space. The Curie-Weiss-like behavior above 100 K in static magnetic- [3,34] and Raman-susceptibilities [17,35,36] suggest A_{2g}pseudovectorlike instabilities at low temperature. Below about 50 K, the Kondo screening begins setting in [16,30,32,34,37] and the correlation length of the HO [38] or LMAF [4,39] phase builds at the ordering vector $Q_0 = (0, 0, 1)$; therefore both the magnetic and Raman uniform susceptibilities start to decrease [Fig. 3]. Close to the transition temperature, both the HO and LMAF order parameters fluctuate regardless of the low temperature ordering [Figs. 1(b)–1(d)]. However, the static magnetic susceptibility at Q_0 diverges only across the PM-LMAF phase transition [4,22], whereas it becomes "near critical" from the PM-HO phase [38]. Thus, HO is a nonmagnetic transition, but there is the "ghost" of LMAF present as shown in Fig. 1(b). Here, we find that the temperature dependencies of the static A_{2g} Raman susceptibility $\chi_{A2g}(0, T)$ are similar and track $\chi_c^m(T)$ in all measured samples, suggesting that the minimal model is applicable for the studied Fe substituted crystals.

We now discuss the origin and the observed doping dependence of the collective mode in the ordered phases within a phenomenological Ginzburg-Landau approach. Within the minimal model, the two order parameters can be constructed from $|A_{2g}\rangle$ and $|A_{1g}\rangle$ [26]. The HO phase was explained as the state in which the two levels mix, resulting in a lower symmetry point group on the uranium site, which breaks all vertical and diagonal reflection symmetry planes, and thus acquires left and right handedness. [17,26] The staggering of left and right handed solutions on the lattice gives rise to the chirality density wave [17] [Fig. 4(a)]. In the HO phase, the staggered condensate can be approximated by a form $|\psi_{\mathrm{HO}}\rangle = \prod_{r=A\ \mathrm{site}} |\mathrm{HO}_r^+\rangle \times \prod_{r=B\ \mathrm{site}} |\mathrm{HO}_r^-\rangle$. Note that $|\mathrm{HO}_r^+\rangle$ at uranium site r is dominantly $|A_{2g}\rangle$, with a small admixture of $|A_{1g}\rangle$, i.e., $|\mathrm{HO}^{\pm}\rangle = \cos\theta |A_{2g}\rangle \pm \sin\theta |A_{1g}\rangle$.

In the HO phase, the orbital mixing is purely real. If, however, the mixing is purely imaginary, the charge distribution on the uranium site does not break any spatial symmetry; instead, it acquires nonzero out-of-plane magnetic moments, and thereby breaks time reversal symmetry. The Néel-type condensate [Fig. 4(b)] takes the form $|\psi_{\mathrm{AFM}}\rangle = \prod_{r=A\ \mathrm{site}} |\mathrm{AFM}_r^+\rangle \times \prod_{r=B\ \mathrm{site}} |\mathrm{AFM}_r^-\rangle$, where $|\mathrm{AFM}^{\pm}\rangle = \cos\theta' |A_{1g}\rangle \pm i \sin\theta' |A_{2g}\rangle$ [26]. The two apparently competing orders, the chirality density wave and the antiferromagnetic state, are both constructed

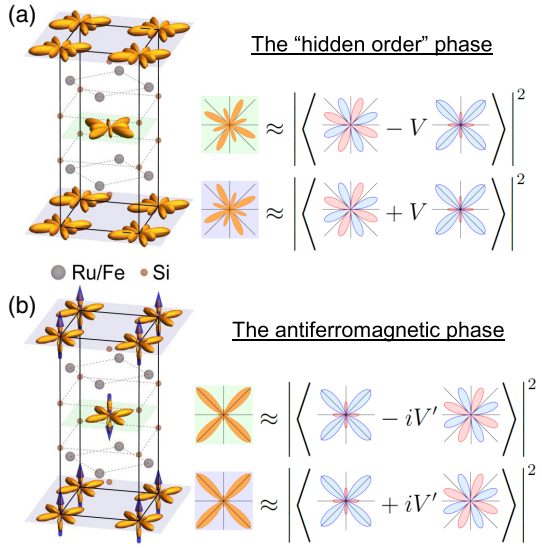

FIG. 4. The crystal structure of $URu_{2-x}Fe_xSi_2$ in (a) the HO and (b) the LMAF phases. Illustrations capturing the symmetries of the charge distributions of the ground state wave functions are placed at the uranium atomic sites. On the right are illustrations showing the in-plane structures of the wave functions. In the HO phase, the crystal field state with the lowest energy has A_{2g} symmetry with 8 nodal lines, $|A_{2g}\rangle$, which mixes with the first excited state with A_{1g} symmetry, $|A_{1g}\rangle$, to form the local wave functions in the HO phase, $|\mathrm{HO}^{\pm}\rangle \approx \cos\theta|A_{2g}\rangle \pm \sin\theta|A_{1g}\rangle$. In the LMAF phase, the ordering of the crystal field states switches, and the new wave functions in the LMAF phase are, $|\mathrm{AFM}^{\pm}\rangle \approx \cos\theta'|A_{1g}\rangle \pm i\sin\theta'|A_{2g}\rangle$. Here, $\theta \equiv \arcsin(V/\omega_0)$ and $\theta' \equiv \arcsin(V'/\omega_0)$, respectively. ω_0 is the splitting between the lowest lying crystal field states in the minimal model. V and V' are the order parameter strength in the HO and LMAF phases, respectively.

by mixing the two orbital wave functions on uranium sites with a real or an imaginary phase factor, $\sin\theta$ or $i\sin\theta'$, thus unifying the two order parameters.

The Ginzburg-Landau free energy can then be constructed from the two component order parameter $\Psi^T \equiv (\psi_{\mathrm{HO}}\, \psi_{\mathrm{AFM}})$, where the order parameters correspond to the two condensates $|\psi_{\mathrm{HO}}\rangle$ and $|\psi_{\mathrm{AFM}}\rangle$ defined above. The free energy takes the form

$$F[\Psi] = \Psi^T \hat{A} \Psi + \beta(\Psi^T\Psi)^2 + \gamma(\Psi^T\hat{\sigma}_1\Psi)^2, \qquad (1)$$

where $\hat{A} \equiv \begin{pmatrix} \alpha_{\mathrm{HO}} & 0 \\ 0 & \alpha_{\mathrm{AFM}} \end{pmatrix}$, with α_{HO} and α_{AFM} vanish at the critical temperature. $\hat{\sigma}_1 \equiv \begin{pmatrix} 0 & 1 \\ 1 & 0 \end{pmatrix}$ is the Pauli matrix. γ controls a finite barrier between the two minima in Figs. 1(e)–1(g), and hence ensures phase separation between the HO and LMAF phases [39]. The free energy parameters are introduced following the recipes given in Haule and Kotliar [27,40] with adjustments to match the phase diagram in Fig. 1(a) [28].

The Ginzburg-Landau free energy in the two dimensional space of ψ_{HO} and ψ_{AFM} is shown in Figs. 1(b)–1(g). Below the second order phase transition, two global and two local minima develop on ψ_{HO} and ψ_{AFM} axes due to spontaneous discrete symmetry breaking, where the minima characterize the ground states in the HO and LMAF phases, respectively.

At the critical doping [Fig. 1(f)], the four minima are degenerate, but the barrier between the minima remains finite due to a γ term in Ginzburg-Landau functional. Therefore the transition between HO and LMAF phases is of the first order, and the coexistence of both phases is allowed, explaining the LMAF puddles that have been observed in the HO phase [41,42].

The energy separation between the dominant long range order (e.g., $|\psi_{\mathrm{HO}}\rangle$) and the subdominant order (e.g., $|\psi_{\mathrm{AFM}}\rangle$) is vanishingly small at the critical Fe concentration, and even away from this point can be smaller than the size of the gap. The exciton of subdominant symmetry (e.g., $|\psi_{\mathrm{AFM}}\rangle$) can form in the gap, which then propagates through the order of the dominant symmetry (e.g., $|\psi_{\mathrm{HO}}\rangle$). Likewise, when the ground state is of $|\psi_{\mathrm{AFM}}\rangle$, the propagating exciton is of $|\psi_{\mathrm{HO}}\rangle$ symmetry. The symmetry difference between the two condensates is A_{2g}; hence, such an exciton can be detected by Raman spectroscopy in the A_{2g} channel, and explains the sharp resonance shown in Fig. 2. It is clear from this discussion that the energy of the resonance vanishes at the critical Fe concentration, and is linearly increasing away from the critical point. For superconductors, such an excitation is known as the Bardasis-Schrieffer mode, characterizing the transition between two competing Cooper pairing channels [43].

More generally, the uranium $5f$ orbitals in solids can arrange in surprising types of orders, including orders with broken chirality or time reversal symmetry. While such orders are competing for the same phase space in URu_2Si_2, they are also subtly connected and were here unified into a common order parameter, which can be switched with small energy cost. The low energy excitations are usually Goldstone modes, but here we detected a new type of excitation, which connects two types of long range order, and is observed as a resonance by light scattering. The resonance brings light to a long-standing problem of emergent phases of exotic local orbital self-organization and their interrelation.

We are grateful for discussions with C. Broholm, N. P. Butch, P. Coleman, I. R. Fisher, P. B. Wiegmann, and V. M. Yakovenko. G. B. and H.-H. K. acknowledge support from DOE BES Grant No. DE-SC0005463. A. L. and V. K. acknowledge NSF Grant No. DMR-1104884. K. H. acknowledges NSF Grant No. DMR-1405303. M. B. M., S. R., and N. K. acknowledge DOE BES Grant No. DE-FG02-04ER46105 (crystal growth) and NSF Grant No. DMR-1206553 (materials characterization).

*hk458@physics.rutgers.edu
†girsh@physics.rutgers.edu

[1] J. S. Hall, M. R. Movassagh, M. N. Wilson, G. M. Luke, N. Kanchanavatee, K. Huang, M. Janoschek, M. B. Maple, and T. Timusk, Electrodynamics of the antiferromagnetic phase in URu_2Si_2, Phys. Rev. B **92**, 195111 (2015).

[2] N. Kanchanavatee, M. Janoschek, R. E. Baumbach, J. J. Hamlin, D. A. Zocco, K. Huang, and M. B. Maple, Twofold enhancement of the hidden-order/large-moment antiferromagnetic phase boundary in the $URu_{2-x}Fe_xSi_2$ system, Phys. Rev. B **84**, 245122 (2011).

[3] S. Ran, C. Wolowiec, I. Jeon, N. Pouse, N. Kanchanavatee, K. Huang, D. Martien, T. DaPron, D. Snow, M. Williamsen *et al.*, Phase diagram and thermal expansion measurements on the system of $URu_{2-x}Fe_xSi_2$, arXiv:1604.00983 [Proc. Natl. Acad. Sci. U.S.A. (to be published)].

[4] N. P. Butch, J. R. Jeffries, S. Chi, J. B. Leão, J. W. Lynn, and M. B. Maple, Antiferromagnetic critical pressure in URu_2Si_2 under hydrostatic conditions, Phys. Rev. B **82**, 060408 (2010).

[5] F. Bourdarot, N. Martin, S. Raymond, L.-P. Regnault, D. Aoki, V. Taufour, and J. Flouquet, Magnetic properties of URu_2Si_2 under uniaxial stress by neutron scattering, Phys. Rev. B **84**, 184430 (2011).

[6] M. Jaime, K. H. Kim, G. Jorge, S. McCall, and J. A. Mydosh, High Magnetic Field Studies of the Hidden Order Transition in URu_2Si_2, Phys. Rev. Lett. **89**, 287201 (2002).

[7] D. Aoki, F. Bourdarot, E. Hassinger, G. Knebel, A. Miyake, S. Raymond, V. Taufour, and J. Flouquet, Field reentrance of the hidden order state of URu_2Si_2 under pressure, J. Phys. Soc. Jpn. **78**, 053701 (2009).

[8] T. T. M. Palstra, A. A. Menovsky, J. van den Berg, A. J. Dirkmaat, P. H. Kes, G. J. Nieuwenhuys, and J. A. Mydosh, Superconducting and Magnetic Transitions in the Heavy-Fermion System URu_2Si_2, Phys. Rev. Lett. **55**, 2727 (1985).

[9] M. B. Maple, J. W. Chen, Y. Dalichaouch, T. Kohara, C. Rossel, M. S. Torikachvili, M. W. McElfresh, and J. D. Thompson, Partially gapped Fermi surface in the heavy-electron superconductor URu_2Si_2, Phys. Rev. Lett. **56**, 185 (1986).

[10] W. Schlabitz, J. Baumann, B. Pollit, U. Rauchschwalbe, H. Mayer, U. Ahlheim, and C. Bredl, Superconductivity and magnetic order in a strongly interacting fermi-system: URu_2Si_2, Z. Phys. B **62**, 171 (1986).

[11] E. R. Schemm, R. E. Baumbach, P. H. Tobash, F. Ronning, E. D. Bauer, and A. Kapitulnik, Evidence for broken time-reversal symmetry in the superconducting phase of URu_2Si_2, Phys. Rev. B **91**, 140506 (2015).

[12] P. Aynajian, E. H. da Silva Neto, C. V. Parker, Y. Huang, A. Pasupathy, J. Mydosh, and A. Yazdani, Visualizing the formation of the Kondo lattice and the hidden order in URu_2Si_2, Proc. Natl. Acad. Sci. U.S.A. **107**, 10383 (2010).

[13] A. R. Schmidt, M. H. Hamidian, P. Wahl, F. Meier, A. V. Balatsky, J. D. Garrett, T. J. Williams, G. M. Luke, and J. C. Davis, Imaging the Fano lattice to 'hidden order' transition in URu_2Si_2, Nature (London) **465**, 570 (2010).

[14] R. Okazaki, T. Shibauchi, H. Shi, Y. Haga, T. Matsuda, E. Yamamoto, Y. Onuki, H. Ikeda, and Y. Matsuda, Rotational symmetry breaking in the hidden-order phase of URu_2Si_2, Science **331**, 439 (2011).

[15] S. C. Riggs, M. C. Shapiro, A. V. Maharaj, S. Raghu, E. D. Bauer, R. E. Baumbach, P. Giraldo-Gallo, M. Wartenbe, and I. R. Fisher, Evidence for a nematic component to the hidden-order parameter in URu_2Si_2 from differential elastoresistance measurements, Nat. Commun. **6**, 6425 (2015).

[16] J. A. Mydosh and P. M. Oppeneer, Colloquium: Hidden order, superconductivity, and magnetism: The unsolved case of URu_2Si_2, Rev. Mod. Phys. **83**, 1301 (2011), and references therein.

[17] H.-H. Kung, R. E. Baumbach, E. D. Bauer, V. K. Thorsmølle, W.-L. Zhang, K. Haule, J. A. Mydosh, and G. Blumberg, Chirality density wave of the "hidden order" phase in URu_2Si_2, Science **347**, 1339 (2015).

[18] Y. J. Jo, L. Balicas, C. Capan, K. Behnia, P. Lejay, J. Flouquet, J. A. Mydosh, and P. Schlottmann, Field-Induced Fermi Surface Reconstruction and Adiabatic Continuity between Antiferromagnetism and the Hidden-Order State in URu_2Si_2, Phys. Rev. Lett. **98**, 166404 (2007).

[19] E. Hassinger, G. Knebel, K. Izawa, P. Lejay, B. Salce, and J. Flouquet, Temperature-pressure phase diagram of URu_2Si_2 from resistivity measurements and ac calorimetry: Hidden order and Fermi-surface nesting, Phys. Rev. B **77**, 115117 (2008).

[20] C. Broholm, J. K. Kjems, W. J. L. Buyers, P. Matthews, T. T. M. Palstra, A. A. Menovsky, and J. A. Mydosh, Magnetic excitations and ordering in the heavy-electron superconductor URu_2Si_2, Phys. Rev. Lett. **58**, 1467 (1987).

[21] T. Williams, H. Barath, Z. Yamani, J. Rodriguez-Riviera, J. Leão, J. Garrett, G. Luke, W. Buyers, and C. Broholm, Gapped excitations in the high-pressure antiferromagnetic phase of URu_2Si_2, arXiv:1607.00967.

[22] P. Das, N. Kanchanavatee, J. S. Helton, K. Huang, R. E. Baumbach, E. D. Bauer, B. D. White, V. W. Burnett, M. B. Maple, J. W. Lynn, and M. Janoschek, Chemical pressure tuning of URu_2Si_2 via isoelectronic substitution of Ru with Fe, Phys. Rev. B **91**, 085122 (2015).

[23] M. N. Wilson, T. J. Williams, Y.-P. Cai, A. M. Hallas, T. Medina, T. J. Munsie, S. C. Cheung, B. A. Frandsen, L. Liu, Y. J. Uemura, and G. M. Luke, Antiferromagnetism and hidden order in isoelectronic doping of URu_2Si_2, Phys. Rev. B **93**, 064402 (2016).

[24] N. P. Butch, S. Ran, I. Jeon, N. Kanchanavatee, K. Huang, A. Breindel, M. B. Maple, R. L. Stillwell, Y. Zhao, L. Harriger, and J. W. Lynn, Distinct magnetic spectra in the hidden order and antiferromagnetic phases in $URu_{2-x}Fe_xSi_2$, arXiv:1607.02136.

[25] T. J. Williams, M. N. Wilson, A. A. Aczel, M. B. Stone, and G. M. Luke, Hidden order signatures in the antiferromagnetic phase of $U(Ru_{1-x}Fe_x)_2Si_2$, arXiv:1607.05672.

[26] K. Haule and G. Kotliar, Arrested Kondo effect and hidden order in URu_2Si_2, Nat. Phys. **5**, 796 (2009).

[27] K. Haule and G. Kotliar, Complex Landau-Ginzburg theory of the hidden order in URu_2Si_2, Europhys. Lett. **89**, 57006 (2010).

[28] See Supplemental Material at http://link.aps.org/supplemental/10.1103/PhysRevLett.117.227601 for details of material growth and data analysis.

[29] D. V. Khveshchenko and P. B. Wiegmann, Raman Scattering and Anomalous Current Algebra in Mott Insulators, Phys. Rev. Lett. **73**, 500 (1994).

[30] W. T. Guo, Z. G. Chen, T. J. Williams, J. D. Garrett, G. M. Luke, and N. L. Wang, Hybridization gap versus hidden-order gap in URu_2Si_2 as revealed by optical spectroscopy, Phys. Rev. B **85**, 195105 (2012).

[31] R. P. S. M. Lobo, J. Buhot, M. A. Méasson, D. Aoki, G. Lapertot, P. Lejay, and C. C. Homes, Optical conductivity of URu_2Si_2 in the Kondo liquid and hidden-order phases, Phys. Rev. B **92**, 045129 (2015).

[32] J. S. Hall, U. Nagel, T. Uleksin, T. Rõõm, T. Williams, G. Luke, and T. Timusk, Observation of multiple-gap structure in hidden order state of URu_2Si_2 from optical conductivity, Phys. Rev. B **86**, 035132 (2012).

[33] M. Sundermann, M. W. Haverkort, S. Agrestini, A. Al-Zein, M. M. Sala, Y. Huang, M. Golden, A. de Visser, P. Thalmeier, L. H. Tjeng *et al.*, Direct bulk sensitive probe of $5f$ symmetry in URu_2Si_2, arXiv:1608.01840.

[34] C. Pfleiderer, J. A. Mydosh, and M. Vojta, Pressure dependence of the magnetization of URu_2Si_2, Phys. Rev. B **74**, 104412 (2006).

[35] S. L. Cooper, M. V. Klein, M. B. Maple, and M. S. Torikachvili, Magnetic excitations and phonon anomalies in URu_2Si_2, Phys. Rev. B **36**, 5743 (1987).

[36] J. Buhot, M.-A. Méasson, Y. Gallais, M. Cazayous, A. Sacuto, G. Lapertot, and D. Aoki, Symmetry of the Excitations in the Hidden Order State of URu_2Si_2, Phys. Rev. Lett. **113**, 266405 (2014).

[37] J. Levallois, F. Lévy-Bertrand, M. K. Tran, D. Stricker, J. A. Mydosh, Y.-K. Huang, and D. van der Marel, Hybridization gap and anisotropic far-infrared optical conductivity of URu_2Si_2, Phys. Rev. B **84**, 184420 (2011).

[38] P. G. Niklowitz, S. R. Dunsiger, C. Pfleiderer, P. Link, A. Schneidewind, E. Faulhaber, M. Vojta, Y.-K. Huang, and J. A. Mydosh, Role of commensurate and incommensurate low-energy excitations in the paramagnetic to hidden-order transition of URu_2Si_2, Phys. Rev. B **92**, 115116 (2015).

[39] P. G. Niklowitz, C. Pfleiderer, T. Keller, M. Vojta, Y.-K. Huang, and J. A. Mydosh, Role of commensurate and incommensurate low-energy excitations in the paramagnetic to hidden-order transition of URu_2Si_2, Phys. Rev. Lett. **104**, 106406 (2010).

[40] L. Boyer and V. Yakovenko, A model for the polar kerr effect in the hidden-order phase of $URu_{2-x}Fe_xSi_2$, APS March Meeting Baltimore Abstracts **R22**, 4 (2016).

[41] K. Matsuda, Y. Kohori, T. Kohara, K. Kuwahara, and H. Amitsuka, Spatially Inhomogeneous Development of Antiferromagnetism in URu_2Si_2: Evidence from ^{29}Si NMR under Pressure, Phys. Rev. Lett. **87**, 087203 (2001).

[42] M. Yokoyama, H. Amitsuka, K. Tenya, K. Watanabe, S. Kawarazaki, H. Yoshizawa, and J. A. Mydosh, Competition between hidden order and antiferromagnetism in URu_2Si_2 under uniaxial stress studied by neutron scattering, Phys. Rev. B **72**, 214419 (2005).

[43] A. Bardasis and J. R. Schrieffer, Excitons and plasmons in superconductors, Phys. Rev. **121**, 1050 (1961).